Chapter-5 Reduced Graphite Oxide and MoS_2 Nanostructures Electrodes for Solid State Supercapacitors

5.1 Introduction

Energy crisis and environmental pollution is increasing to a serious level due to continuous use of fossil fuels and hence that there is need of lightweight, low-cost, eco-friendly, and adaptable efficient energy storage systems. Supercapacitors are widely employed in different applications such as automobiles, electronic gadgets, and hybrid power sources due to their ultra-high power density, quick charging capability, exceptionally long cycle life, and operational safety [228,229]. In order to maximise the usability of the supercapacitor devices for consumer applications, there is a need for producing compact supercapacitors that operate over a wide voltage range. Thus, solid-state supercapacitors are chosen as prospective wearable devices which can provide fast charging of consumer device with high cyclic stability compared to batteries and fuel cells [230,231]. A conventional supercapacitor typically has different configuration, such as coin type, cylindrical, and flexible assembles, as shown in **Figure 5.1**. The major components are two electrodes and an electrolyte-saturated separator, which are placed in a conductive metal case during coin cell manufacturing and the assemble is sealed under high pressure to prevent leakage and sorting of cell (**Figure 5.1 a**). The coin-cell design is ideal for powering compact devices. The cylindrical cell design of supercapacitor is also used in commercial purpose. This design consists of rolling layers of electrode and separator sheets packed in metal casing to enhance the mechanical durability, as shown in **Figure 5.1 b**. **Figure 5.1 c** depicts an alternative design known as the flexible supercapacitor assemble (pouch cell), which likewise uses layer-by-layer flexible sheets of electrodes and separators.

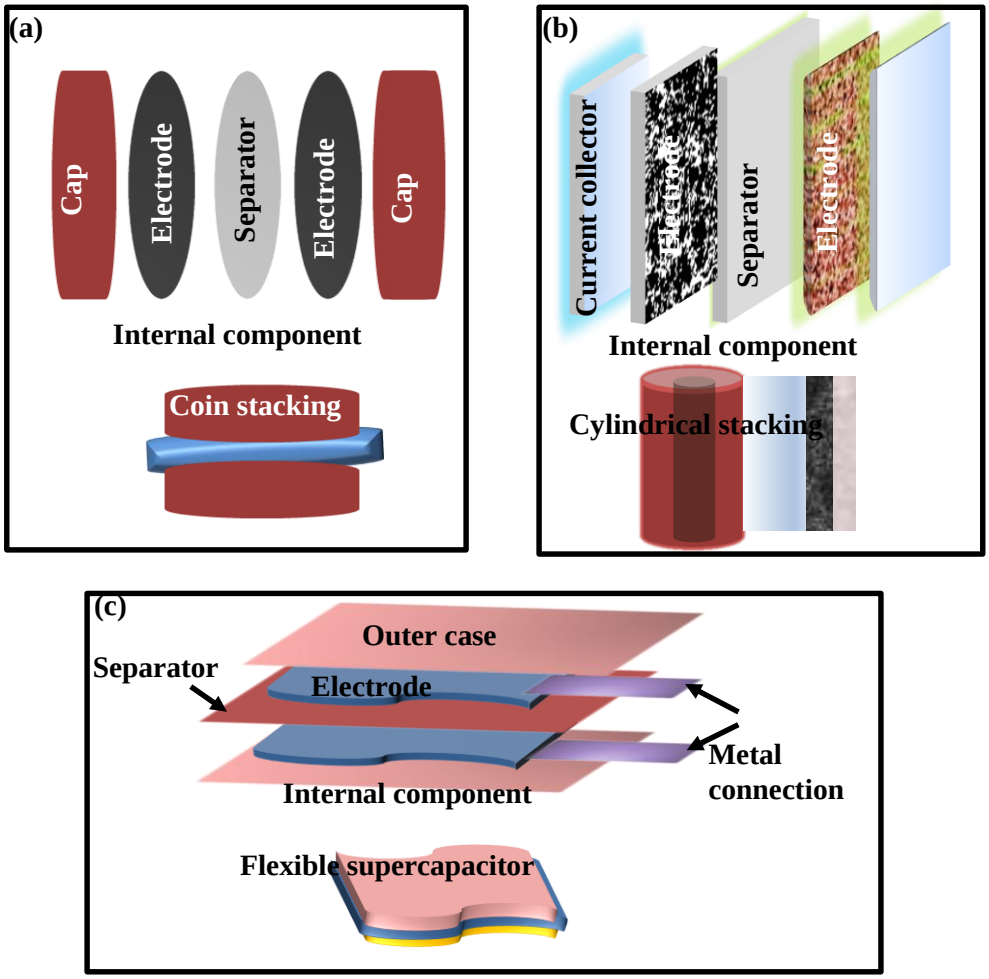

Figure 5.1 *Schematic for different types of supercapacitor (a) coin type, (b) stack rectangular, and (c) flexible assembles.*

The active materials (or electrode materials) and electrolytes are essential and significant constituent in supercapacitors and plays a crucial role. Active materials are responsible for charge storage in supercapacitors via ion adsorption and/or redox reactions. The electrode material should be low-cost and ecologically benign. Faradic charge transfer capacity of electrode also plays important role in improving the capacitance. Carbon materials have been vigorously used in supercapacitors due to their high conductivity, large specific surface area (up to 2000 m^2 g^{-1}), strong corrosion resistance, regulated porosity structure and chemical stability. Among carbon materials, reduced graphite oxide (rGO) has been widely exploited for supercapacitor electrodes. Electrolyte is another crucial

component in the construction of supercapacitor, since the highest operational voltage is determined by the breakdown voltage of the electrolyte which determines the energy density of supercapacitors. A suitable electrolyte should possess a wide operating voltage window, good electrochemical stability, high ionic concentration, low resistivity, non-toxicity with low cost. The aqueous electrolyte-based supercapacitors have the possibility of leaking, which grows as the life cycle progresses. So, they must be well-encapsulated and handled and stored with care. The ionic liquids have advantage of higher voltage window, but their toxicity, preparation and high cost make them unsuitable for commercial use. As a result, the use of these electrolytes limits the range of supercapacitor applications. The solid electrolyte acts as both electrolyte and separator and avoid short circuit and chemical leakage. Polymer gel electrolytes are easy to manufacture, offer a high level of safety, are mechanically flexible, and lightweight. So, compared to liquid counterparts, solid-state supercapacitors (SSC) are much safer and more suitable for commercial applications. Gel polymers are a mixture of solid polymers and liquid electrolytes that are formulated to sustain the ionic conductivity of the liquid electrolyte and mechanical strength of polymer.

Wu *et al.* synthesized nitrogen and boron co-doped monolithic graphene aerogel based solid-state supercapacitor (SSC) using PVA/H_2SO_4 as solid-state electrolyte showing lower value of energy density around 8.65 Wh kg^{-1} [232]. Similarly, Wang *et al.* manufactured flexible SSC using electrophoretic deposition of graphene on carbon cloth. The fabricated SSC device shows specific capacitance of 79.19 F g^{-1} but it suffers with low energy density~ 1.64 Wh kg^{-1} [233]. Moreover, recently MoS_2 nanostructures have also gained much attention as potential supercapacitor electrode materials due to their ultrathin layer structure which provide suitable surface area for double-layer charge storage. The centre molybdenum atoms of the lamellar structure possess high potential for

pseudocapacitance and promote charge storage due to its variable oxidation states (from +2 to +6). Also, the weak intermolecular van der Waals interactions between the layers allows proper electrolyte diffusion and structural rigidity resulting in high electrochemical stability [211,212]. There are very few studies only on MoS_2 nanostructures based SSC devices. Joseph *et al.* demonstrated metallic 1T- MoS_2 based SSC device with high energy density of 21.35 W h kg^{-1}, the cell deliver maximum specific capacitance of 68.9 F g^{-1} at current density of 1 A g^{-1} [234]. Zhou *et al.* developed a vertical MoS_2 nanosheets array-based SSC with a specific capacitance of 80.1 F g^{-1} at 1 A g^{-1} and a maximum energy density of 11.13 W h kg^{-1} [235]. In the present chapters, the common electrochemical methods like CV, GCD, EIS and stability studies have been discussed for fabricated SSC devices using rGO and MoS_2 nanostructures electrodes. There have been very few studies on rGO and MoS_2 as electrodes for solid state supercapacitors. The comparative study of these materials with acidic and basic solid electrolyte is still lacking for solid state supercapacitor.

5.2 Results and Discussion

In the present work, we have demonstrated hydrothermally prepared reduced graphite oxide, hexagonal phase of MoS_2 nanostructures (nanosheets and nanoflowers) and MoS_2-rGO-NS heterostructure as electrode material for SSC device with neutral (PVA-Na_2SO_4) and acidic (PVA-H_2SO_4) solid electrolyte membranes. We have fabricated the SSC devices with coating of active material on 2 cm ×2 cm area of conducting carbon paper and evaluated their capacitive performance. The specific capacitance of SSC device using CV curves can be determined by following **equation 5.1**-[236]

$$C_s = \frac{\textit{Area under the cyclic voltammetry curve}}{\textit{Mass of electrode material} \times \textit{Potential window} \times \textit{Voltage scan rate}} \qquad (5.1)$$

In GCD measurement, supercapacitor is charged and discharged in constant current within a potential range. The specific capacitance (C_s) value can be calculated using **equation 5.2**-

$$C_s = \frac{Current \times Discharge\ time}{Todal\ mass\ of\ active\ material\ at\ both\ electrodes \times Potential\ window} \quad (5.2)$$

The energy density (E) and power density (P) of SSC device can be computed using the GCD curves as per following **equations 5.3** and **5.4** [237,238]-

$$E = \frac{1}{2}\frac{C_s(\Delta V)^2}{3.6} \quad (5.3)$$

$$P = \frac{E*3600}{\Delta t} \quad (5.4)$$

where C_s is specific capacitance obtained from GCD, **Δ**V is potential difference and **Δ**t is discharge time calculated from GCD curve.

5.2.1 Reduced Graphite Oxides Based Solid State Supercapacitors

In this study, we have investigated the capacitive performance of hydrothermally synthesized rGO-HH and rGO-Urea SSC devices with acidic solid electrolyte by performing electrochemical measurements. The electrochemical studies of rGO-HH and rGO-Urea SSC devices have been performed with PVA-H_2SO_4 electrolyte in voltage range of -0.7 to 0.7 V. **Figure 5.2 (a)** shows the photograph of designed SSC device. **Figure 5.2 (b)** shows the CV curves for rGO-HH SSC device at different voltage scan rates ranging from 5 to 100 mV s^{-1}. The presence of some degree of redox behaviour in CV curves for rGO-HH SSC implies the existence of pseudo behaviour along with EDLC at electrode/electrolyte interface in symmetric cell, which is similar to observed behaviour in three cell measurement. The specific capacitance value of SSC device has been calculated by **equation 5.1**. The specific capacitance values of 46, 44, 44, 41 and 35 F g^{-1} are obtained for rGO-HH SSC device at scan rates of 5, 10, 20, 50 and 100 mV s^{-1}, respectively. Further,

we have performed the GCD measurements for better understanding and quantitative insight of charging discharging capability of device. **Figure 5.2 (c)** displays the GCD curves for rGO-HH SSC device at varied current densities from 0.2 to 2 A g^{-1}, which maintains the quasi-triangular behaviour. The specific capacitance from GCD curves can be calculated using **equation 5.2**. The specific capacitance of 35 F g^{-1} for full cell has been observed at discharge current density of 0.2 A g^{-1}. The specific capacitances of 31, 28, and 25 F g^{-1} are obtained at discharge current density of 0.5, 1 and 2 A g^{-1}, respectively.

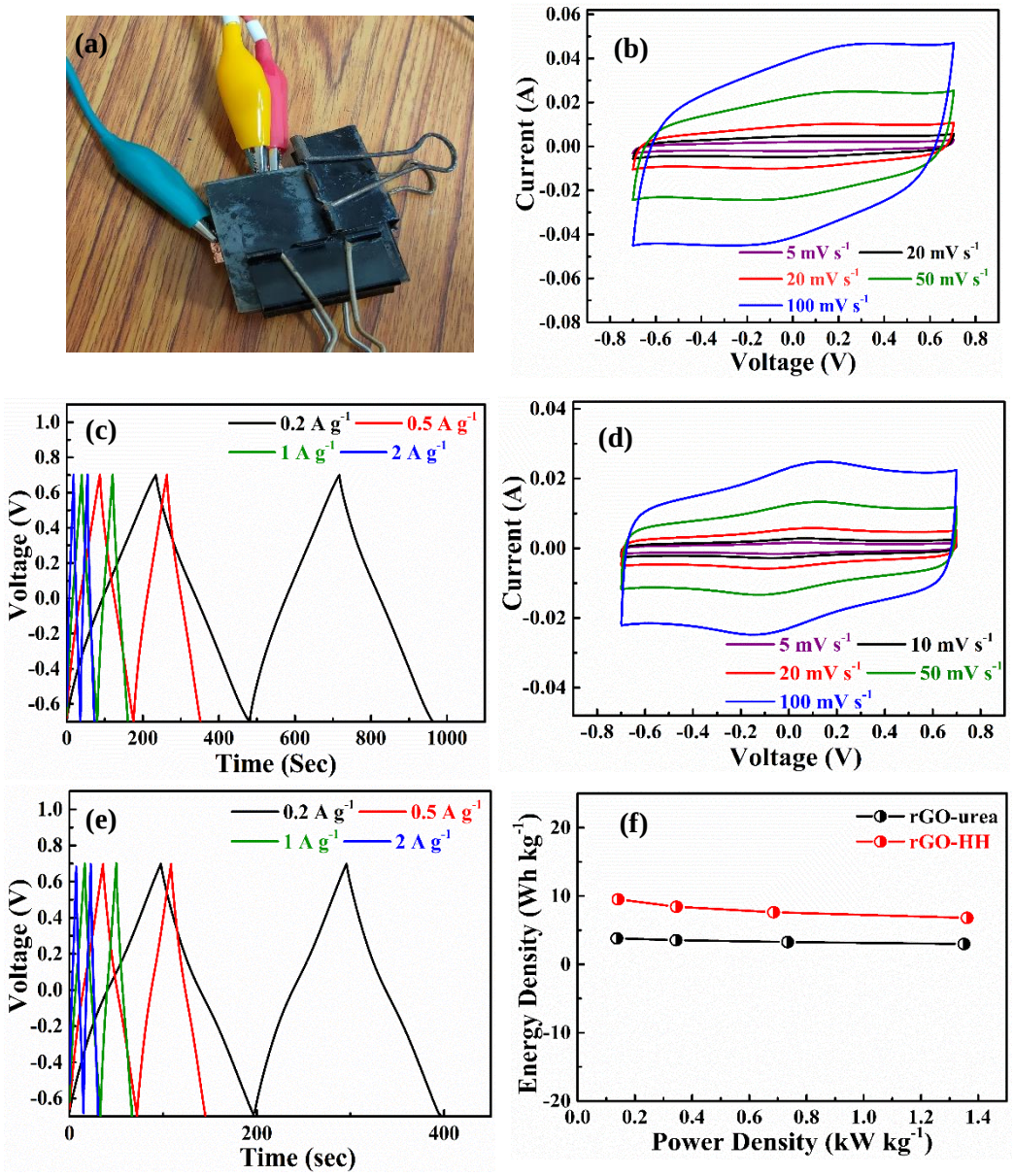

Figure 5.2 *(a) Photograph of designed SSC device, (b) CV curves at varied voltage sweep rates, and (c) GCD curves at different discharge current densities for rGO-HH based SSC device, (d) CV curves at varied voltage sweep rates and (e) GCD curves at different discharge current densities for rGO-Urea based SSC, and (f) Energy density vs power density curves for both SSC devices with acidic solid electrolyte.*

Figure 5.2 (d) and **(e)** represent capacitive behaviour of rGO-Urea SSC device. **Figure 5.2 (d)** shows CV curves of rGO-Urea SSC device showing maximum specific capacitance of 27 F g^{-1} at sweep rate of 5 mV s^{-1}. The specific capacitances of 25, 25, 24 and 22 F g^{-1} are obtained at voltage sweep rates of 10, 20, 50 and 100 mV s^{-1} for SSC device. The GCD curves of rGO-Urea SSC in acidic electrolyte are shown in **Figure 5.2 (e)**, suggesting maximum specific capacitances of 14 F g^{-1} at discharge current density of 0.2 A g^{-1}. The specific capacitances of 13, 12, and 11 F g^{-1} are obtained at discharge current densities of 0.5, 1 and 2 A g^{-1}, respectively. Further, energy density and power density of rGO-HH and rGO-Urea SSC devices have been evaluated with acidic (PVA-H_2SO_4) electrolyte**,** as shown in **Figure 5.2 (f)**. The energy density (E) and power density (P) of designed SSC device are determined using **equations 5.3** and **5.4**. The maximum energy densities of 9.5 and 3.8 W h kg^{-1} are observed at power density of 0.141 kW kg^{-1} and 0.137 kW kg^{-1} for rGO-HH and rGO-Urea SSC devices, respectively. It clearly suggests that rGO-HH SSC device possess higher energy density at larger power density compared to rGO-Urea based SSC device.

To further understand the kinetics at electrode/electrolyte interface, we have performed EIS study of fabricated SSC devices and corresponding Nyquist plots are given in **Figure 5.3 (a)** with equivalent circuit as inset. The elements in the equivalent circuit include resistance of the solid electrolyte and cell components (R_s), charge transfer resistance (R_{ct}), constant phase element (CPE) and Warburg impedance (W) [239,240]. The inset shows the low internal resistance (R_s ~ 0.95 Ω) for rGO-HH based SSC device compared to rGO-Urea based SSC device (R_s ~14.2 Ω). The rate of redox reactions at

electrode/electrolyte interface is determined using charge transfer resistance (R_{CT}). The smaller charge transfer resistance for rGO-HH SSC (R_{CT}~ 2.6 Ω) compared to rGO-Urea one (96.18 Ω) indicates faster electron transfer at electrode/electrolyte interface leading to better performance of rGO-HH SSC device. **Figure 5.3 (b)** shows Bode impedance plots (log |Z| vs. log f), which followed the trend of Nyquist plot and provides the direct view of impedance (modulus) for each frequency range. It clearly indicates the low value of |Z| for rGO-HH SSC compared to rGO-Urea one suggesting good conducting behaviour of rGO-HH in acidic electrolyte, as observed in three cell measurement.

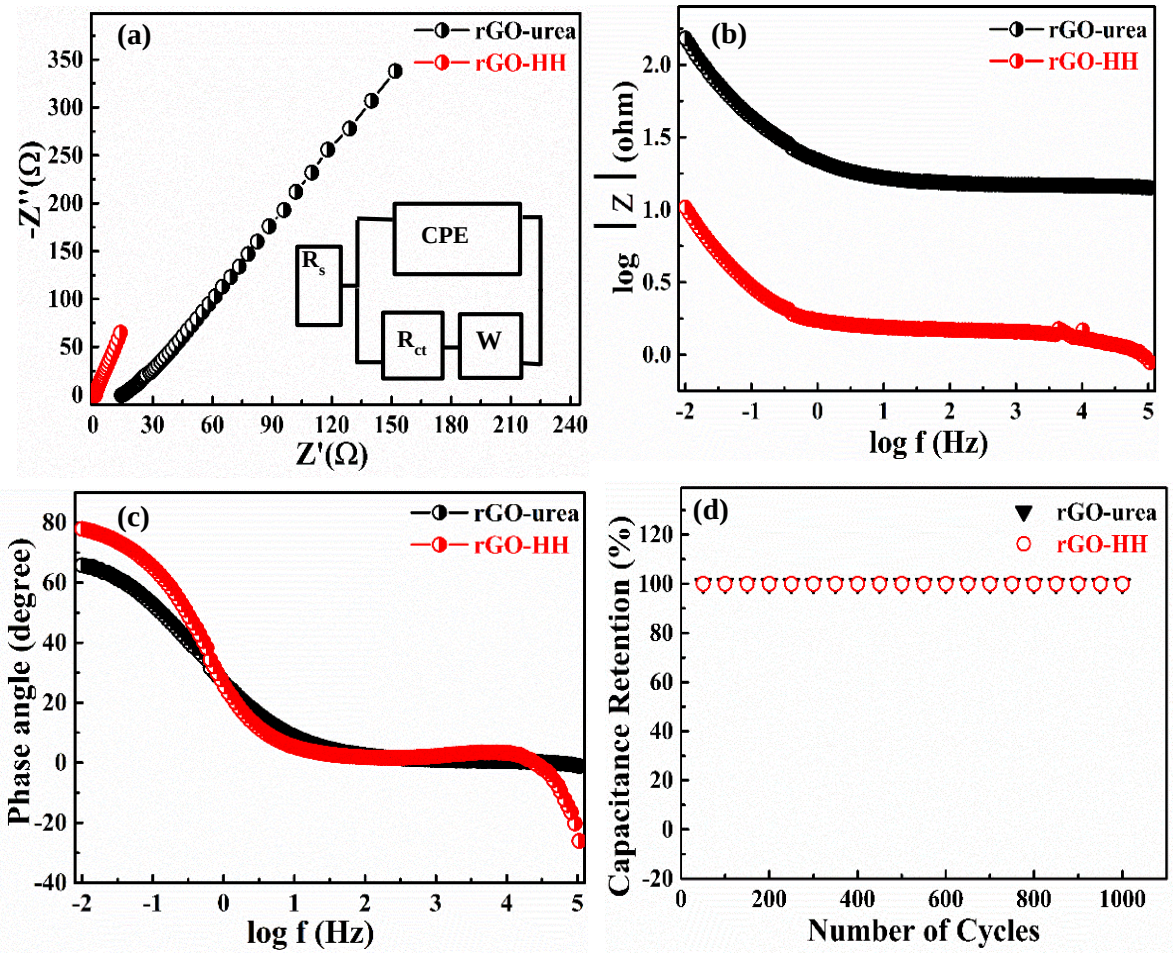

Figure 5.3 *(a) Nyquist plots (inset shows the equivalent circuit), (b) Bode impedance modulus plots, (c) Bode phase angle plots, and (d) Cyclic stability test at discharge current density of 2 A g^{-1} for rGO-HH and rGO-Urea based SSC devices.*

The Bode phase plots of **Figure 5.3 (c)** shows the maximum phase angle of 78° and 66° for rGO-HH and rGO-Urea SSC devices with acidic electrolyte, indicating the presence

of pseudocapacitive behaviour along with EDLC for both SSC devices. The pseudocapacitive behaviour is observed due to the presence of oxygen containing functional groups in both rGO samples. Additionally, the cyclic stability of capacitive performance of rGO-HH and rGO-Urea SSC devices is tested for 1000 cycles as shown in **Figure 5.3 (d)**, which shows nearly 100% capacitance retention after 1000 cycles, suggesting higher degree of stability of as fabricated SSC device. In summary, a comparative study of capacitive performance of hydrothermally synthesized rGO-HH and rGO-Urea solid state supercapacitor devices have been performed in the present work. The utilization of polymer gel electrolyte in solid-state supercapacitors increases the voltage window and hence the energy density. The rGO based SSC devices have not been explored with neutral solid electrolyte as rGO sample have poor capacitive response in neutral electrolyte.

5.2.2 MoS_2 Nanoflowers Based Solid State Supercapacitors

This section deals with the electrochemical characterization and investigation of capacitive performance of hydrothermally synthesized MoS_2 nanoflowers SSC device with neutral and acidic electrolytes. To examine the practical performance, we studied the capacitive response of MoS_2 nanoflowers SSC device in voltage range -0.8 to 0.8 V for neutral (PVA-Na_2SO_4) and -0.7 to 0.7V for acidic (PVA-H_2SO_4) solid electrolytes. **Figure 5.4 (a)** shows the SEM image of MoS_2 nanoflowers depicting formation of petals with exposed edges, while **Figure 5.4 (b)** shows the CV curves for designed SSC at different voltage scan rates from 5 to 100 mV s^{-1} with neutral electrolyte. The deviation from rectangular behaviour in CV curves for MoS_2 nanoflowers SSC device implies the presence of electric double-layer and pseudocapacitance in symmetric cell. The specific capacitance value of SSC device has been calculated using **equation 5.1**. The specific capacitance of 56, 54, 41, 27 and 21 F g^{-1} is obtained for full cell at scan rates of 5, 10, 20, 50 and 100 mV

s^{-1} for SSC device. **Figure 5.4 (c)** displays the GCD curves for SSC device with neutral electrolyte at varied current densities from 0.2 to 2 A g^{-1}, which maintain the quasi-triangular behaviour again indicating the presence of double layer formation along with pseudocapacitance. The specific capacitances of 46.5, 34, 22, and 13 F g^{-1} are obtained at discharge current density of 0.2, 0.5, 1 and 2 A g^{-1}, respectively.

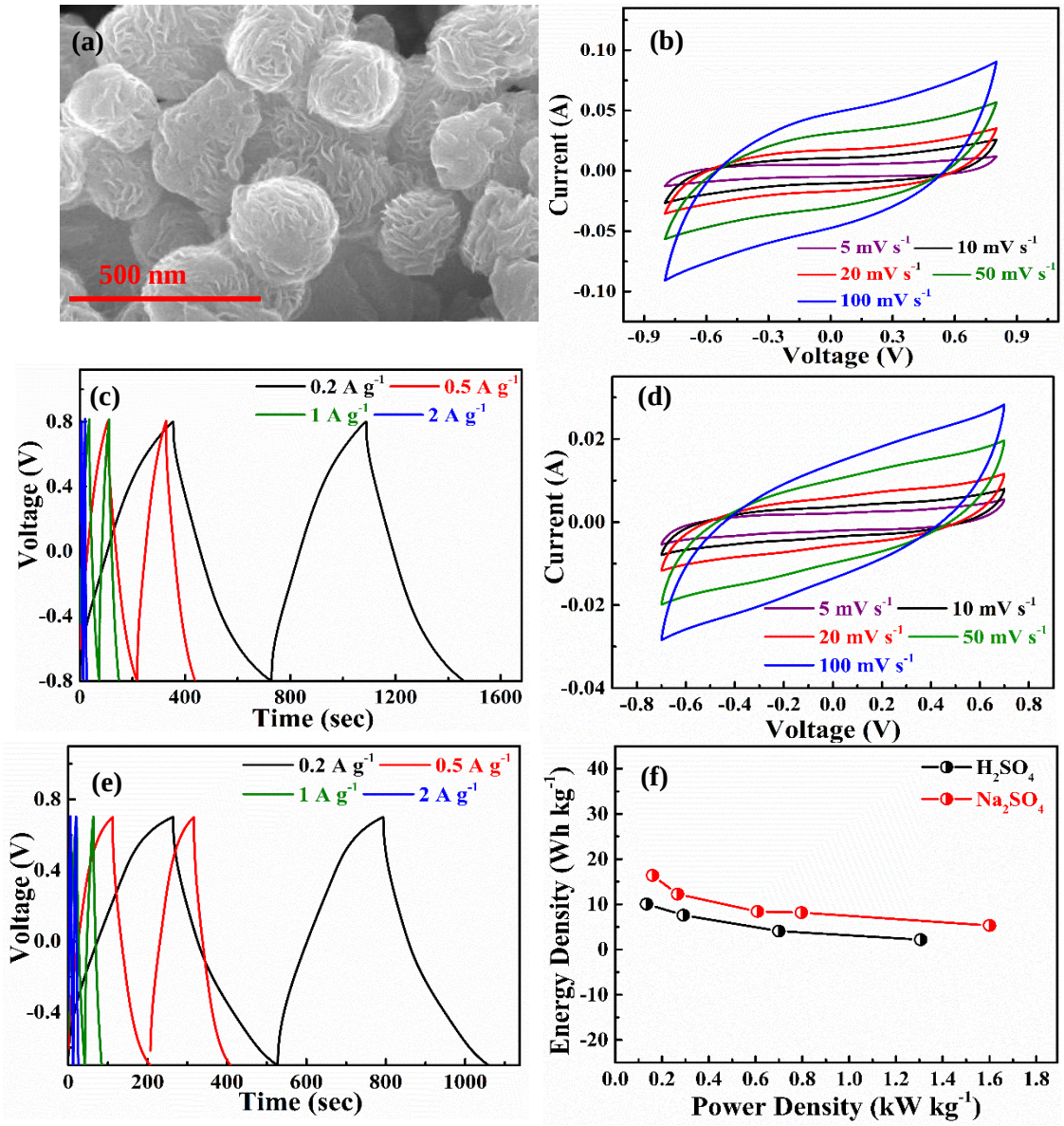

Figure 5.4 *Electrochemical measurements for MoS_2 nanoflowers based SSC devices (a) SEM Image of MoS_2 nanoflowers, (b) CV curves at varied sweep rates, and (c) GCD curves at different discharge current densities with neutral electrolyte, (d) CV curves at varied sweep rates, and (e) GCD curves at different discharge current densities with acidic electrolyte, (f) Energy density vs power density plot for SSC device with both electrolytes.*

Figure 5.4 (d) and **(e)** represent capacitive response of SSC device with acidic electrolyte. The CV curves of **Figure 5.4 (d)** for MoS_2 nanoflowers SSC device show maximum specific capacitances of 52, 47, 40, 32 and 19 F g^{-1} has been obtained at voltage sweep rates of 5, 10, 20, 50 and 100 mV s^{-1}, respectively. The GCD curves of SSC device with acidic electrolyte are shown in **Figure 5.4 (e)**, indicating pseudocapacitive behaviour with specific capacitances of 38, 33, 15 and 9 F g^{-1} at discharge current densities of 0.2, 0.5, 1 and 2 A g^{-1}, respectively. **Figure 5.4 (f)** depicts the high sustainability of energy density of SSC device at high power densities for both neutral and acidic electrolytes. The energy density (E) and power density (P) of designed SSC device is determined using following **equations 5.3** and **5.4** with both neutral and acidic electrolytes. The maximum energy densities of 16.4 and 10 W h kg^{-1} are observed at power densities of 0.159 kW kg^{-1} and 0.134 kW kg^{-1} for neutral and acidic electrolytes, respectively. The observation of high energy densities at high power densities suggests excellent sustainability of capacitive response for MoS_2 nanoflowers SSC device. The EIS measurements of the SSC device with both electrolytes are carried out and corresponding CPE fitted Nyquist plots and equivalent circuit are given in **Figure 5.5 (a)**. The presence of semicircle at higher frequencies and a straight line nearly parallel to the imaginary axis in lower frequency region confirms the good capacitive behaviour of designed SSC. The inset shows the internal resistance, R_s ~ 0.7 Ω and 17 Ω, while charge transfer resistance, R_{ct} ~ 11 Ω and 33.0 Ω for SSC device with acidic and neutral electrolytes, respectively. **Figure 5.5 (b)** shows the Bode impedance plots, which clearly indicates low value of |Z| for both neutral and acidic electrolyte, suggesting good conducting behaviour of MoS_2 nanoflowers based SSC device. The Bode phase plots of **Figure 5.5 (c)** show the maximum phase angle ~ 56° and 50° for acidic and neutral electrolytes, respectively, indicating the presence of redox reactions (pseudocapacitive behaviour) along with double layer capacitance for both electrolytes.

The oxygen containing functional groups and exposed petal edges are responsible for the faradaic redox reactions in MoS_2 nanoflowers.

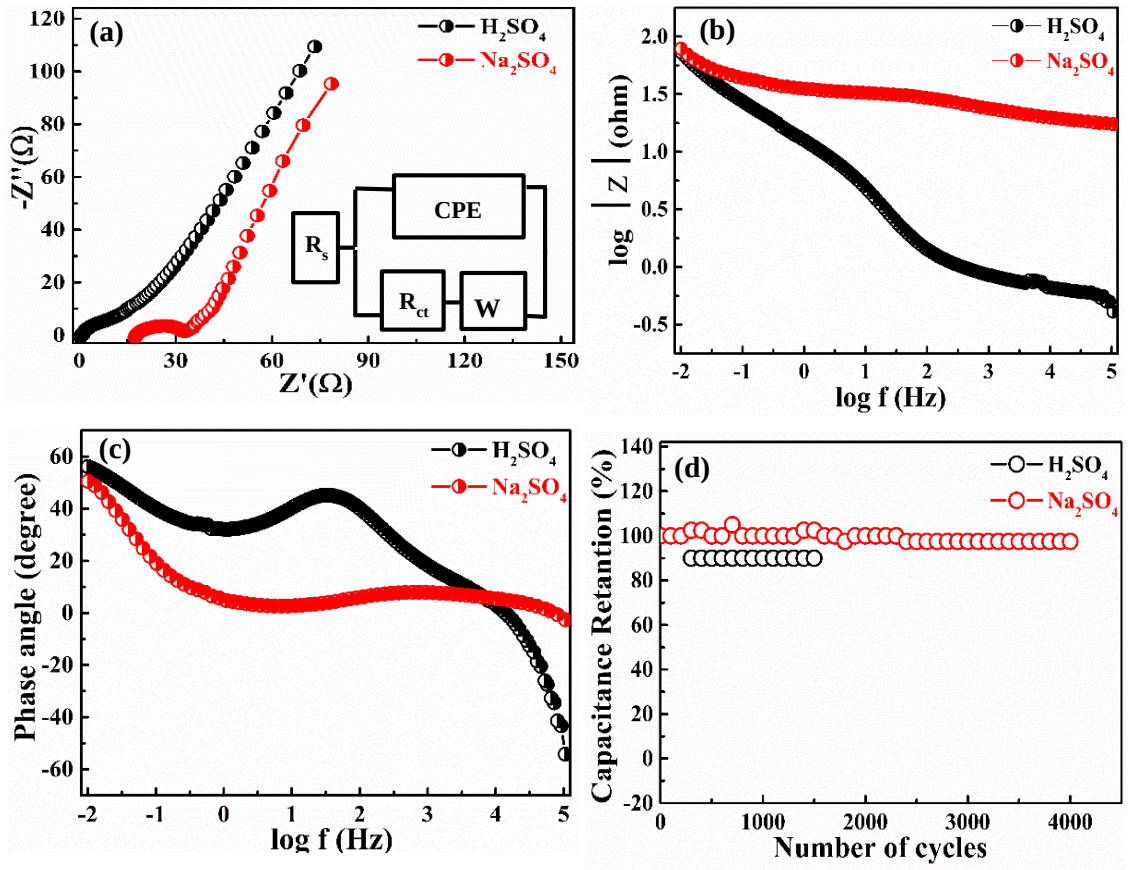

Figure 5.5 *(a) Nyquist plots (inset shows the equivalent circuit), (b) Bode impedance plots, (c) Bode phase angle plots, and (d) Cyclic stability test at discharge current density of 2 A g^{-1} for MoS_2 nanoflowers based SSC device with neutral and acidic solid electrolytes.*

Additionally, the cyclic stability of capacitive performance of SSC device is tested for 4000 and 1500 cycles with neutral and acidic electrolytes, respectively, as shown in **Figure 5.5 (d)**. The capacitance retentions of ~ 97.5% and 90% have been observed with neutral and acidic electrolyte, respectively, suggesting higher degree of stability of prepared MoS_2 nanoflowers based SSC device with neutral electrolyte. In summary, we demonstrate a high capacitive performance and along with good cyclic stability of 2H phase MoS_2 nanoflowers SSC device with both acidic and neutral electrolyte. The use of a polymer gel-electrolyte allows higher voltage window and hence higher energy, and power outputs are

achieved for SSC device. The present work suggests the improved electrochemical performance of 2H-MoS_2 nanoflowers based SSC device, which can be directly attributed to its large accessible surface area due to petals formation and presence of oxygen containing functional groups facilitating the charge transport.

5.2.3 MoS_2 Nanosheets Based Solid State Supercapacitors

This section deals with the electrochemical characterization and investigation of capacitive performance of hydrothermally synthesized MoS_2 nanosheets based SSC devices. The CV, GCD and EIS studies have been performed to investigate the capacitive behaviour of MoS_2 nanosheets electrode SSC device. To determine practical feasibility, the capacitive behaviour of MoS_2 nanosheets solid state supercapacitor (SSC) device with neutral (PVA-Na_2SO_4) and acidic (PVA-H_2SO_4) electrolytes has been investigated in voltage range -0.8 to 0.8 V for neutral and -0.7 to 0.7V for acidic electrolytes.

SEM image of **Figure 5.6 (a)** displays the wrinkled sheets morphology of MoS_2, whereas the inset image shows the photograph of series combination of two MoS_2 nanosheets SSC devices demonstrating lighting up of light emitting diode. **Figure 5.6 (b)** depicts the corresponding CV curves of MoS_2 nanosheets SSC device at varied voltage sweep rates from 5 to 100 mV s^{-1} with PVA-Na_2SO_4 electrolyte. The CV curves seem to maintain quasi rectangular shape, indicating the electric double-layer formation at electrode/electrolyte interface along with pseudocapacitance in SSC device. The shape of the CV curves does not change with increasing sweep rates, implying good rate capability and remarkable capacitive behaviour of SSC with neutral electrolyte. The specific capacitance value of SSC device has been calculated using **equation 5.1**. The MoS_2 nanosheets based SSC device shows maximum specific capacitance of 101 F g^{-1} for full cell at a sweep rate of 5 mV s^{-1}. The specific capacitances of 85, 72, 54 and 39 F g^{-1} are obtained at voltage sweep rate of 10, 20, 50 and 100 mV s^{-1} for SSC device. The decrement

in specific capacitance value with increasing scan rates is seen owing to charge resistive behaviour of MoS_2 electrode material at higher sweep rate. The enhanced capacitive performance of SSC is due to the presence of edges and functionality which facilitates the ion adsorption at electrode/electrolyte interface indicating some degree of pseudocapacitance. **Figure 5.6 (c)** displays the GCD curves for MoS_2 nanosheets based SSC with neutral electrolyte at varied current densities from 0.2 to 2 A g^{-1}. The symmetric triangular shapes of all GCD curves suggests good capacitive behaviour of SSC device. The specific capacitances of 101, 62, 50 and 31 F g^{-1} are obtained at discharge current density of 0.2, 0.5, 1 and 2 A g^{-1}, respectively. **Figure 5.6 (d)** and **(e)** represent capacitive behaviour of SSC device with PVA-H_2SO_4 electrolyte. The CV curves of **Figure 5.6 (d)** diverge from its symmetric rectangular shape, which implies the possibility of cation intercalation and reversible redox reactions at the interface of electrode/electrolyte. The maximum specific capacitance of 88 F g^{-1} has been obtained at sweep rate of 5 mV s^{-1}, which is lower compared to neutral electrolyte. The specific capacitances of 65, 46, 39 and 21 F g^{-1} are obtained at voltage sweep rate of 10, 20, 50 and 100 mV s^{-1} for SSC device.

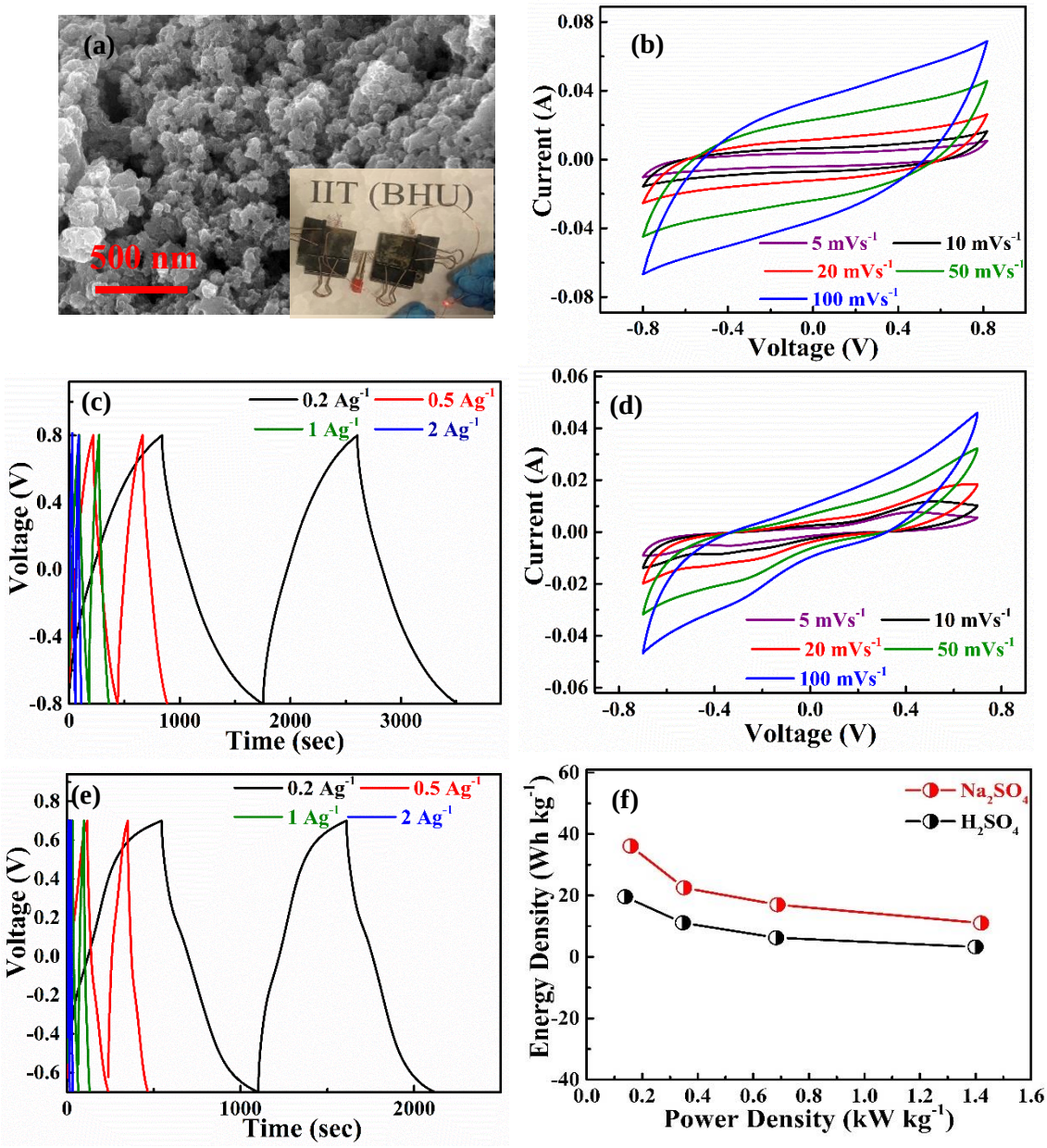

Figure 5.6 *Electrochemical measurements for MoS_2 nanosheets based SSC device (a) SEM image of MoS_2 nanosheets with inset showing series connection of two SSC devices to light up the LED, (b) CV curves at varied sweep rates, and (c) GCD curves at different discharge current densities with neutral electrolyte, (d) CV curves at varied sweep rates, and (e) GCD curves at different discharge current densities with acidic electrolyte, (f) Energy density vs power density plot for MoS_2 nanosheets based SSC device with both electrolytes.*

We have performed the GCD measurements of device for better understanding and quantitative insight of charging discharging capability in acidic electrolyte as shown in **Figure 5.6 (e)**, which shows pseudocapacitive behaviour induced by redox reactions contribution at electrode/electrolyte interface. The specific capacitances of 72, 41, 23 and

12 F g^{-1} are obtained at discharge current densities of 0.2, 0.5, 1 and 2 A g^{-1}, respectively. Further, energy density (E) and power density (P) of designed SSC device are determined using **equations 5.3** and **5.4**. The maximum energy densities of 36.1 and 19.6 W h kg^{-1} are observed at power densities of 0.158 kW kg^{-1} and 0.138 kW kg^{-1} for neutral and acidic electrolyte, respectively. **Figure 5.6 (f)** depicts the high sustainability of energy density for MoS_2 nanosheets based SSC device at high power densities for both neutral and acidic electrolytes. The high sustainable energy density of SSC device based on MoS_2 nanosheets could be due to its morphology and functional groups that provide ultrafast transportation of ion.

To further understand the kinetics at electrode/electrolyte interface, we have performed EIS study of SSC device with both electrolytes and corresponding Nyquist plots are given in **Figure 5.7 (a)** with equivalent circuits as inset. It shows low internal resistance R_s ~ 2.2 Ω and 1.7 Ω and charge transfer resistance, R_{ct} ~ 25 Ω and 48 Ω for SSC device with neutral and acidic electrolytes, respectively. The low value of charge transfer resistances with neutral electrolyte leads to the excellent capacitive behaviour of MoS_2 nanosheets based SSC device. **Figure 5.7 (b)** shows Bode impedance plots, which follow the trend of Nyquist plot and provide the direct view of impedance in varying frequency range. It clearly indicates low value of |Z| for both electrolytes suggesting good conducting behaviour of MoS_2 nanosheets based SSC device. The Bode phase plots of **Figure 5.7 (c)** shows the maximum phase angle ~ 53° and 47° for neutral and acidic electrolytes, indicating the dominance of redox reaction (pseudocapacitive behaviour) over EDLC in SSC for both electrolytes. The oxygen containing functional groups are responsible for the faradaic redox reactions.

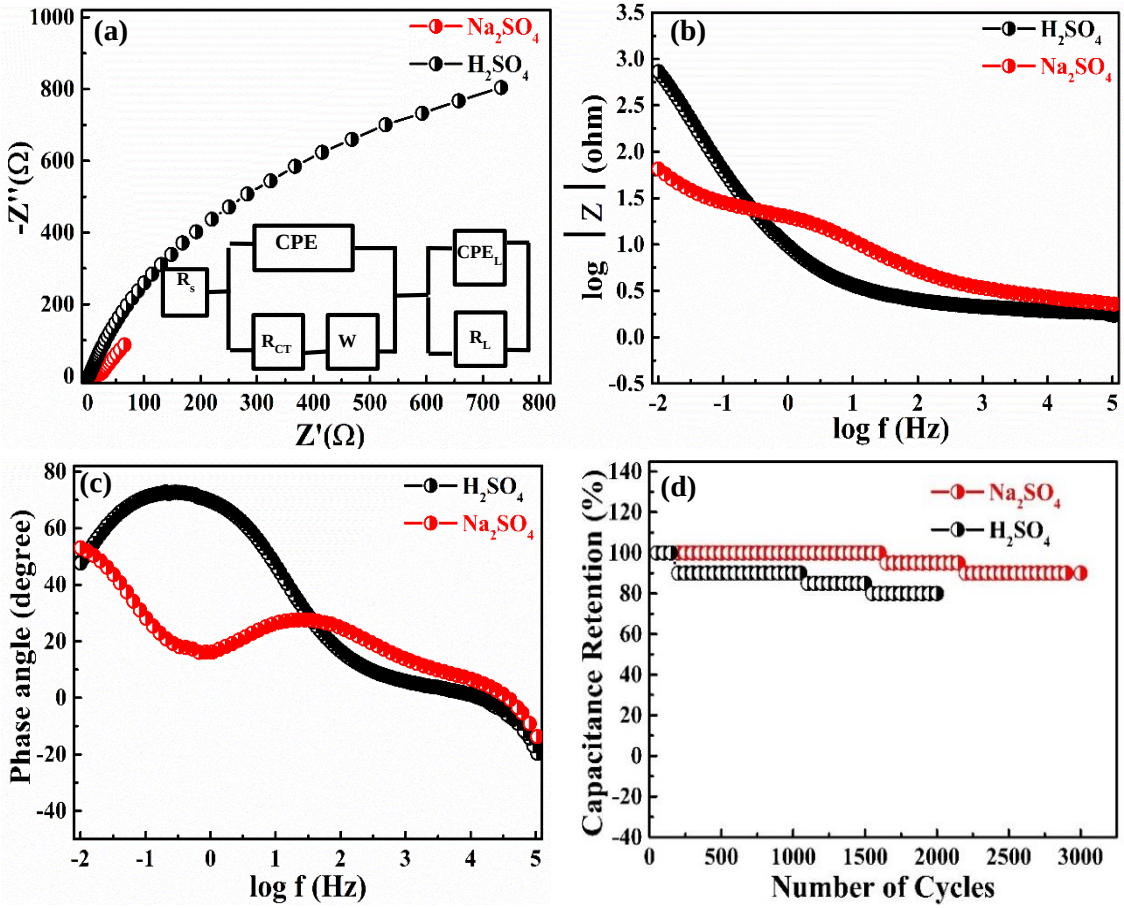

Figure 5.7 *(a) Nyquist plots (inset shows the equivalent circuit), (b) Bode impedance plots, (c) Bode phase angle plots and (d) Cyclic stability test of SSC device at discharge current of 2 A g^{-1} for MoS_2 nanosheets based SSC device with both electrolytes.*

Additionally, the cyclic stability of capacitive performance of SSC device is tested for 3000 and 2000 cycles with neutral and acidic electrolytes, respectively, as shown in **Figure 5.7 (d)**. The capacitance retentions of ~ 90% and 80% have been observed with neutral (3000 cycles) and acidic (2000 cycles) electrolytes, respectively, suggesting higher degree of stability of prepared MoS_2 nanosheets based SSC device with neutral electrolyte. In summary, the electrochemical study verifies that the prepared 2H phase MoS_2 nanosheets based SSC device show good capacitive response along with excellent cyclic stability with both acidic and neutral electrolyte. The utilization of polymer gel- electrolyte provides wider operational voltage window and hence leading to high energy densities of 36 and 19.6 Wh kg^{-1} for fabricated SSC device with neutral and acidic solid electrolyte,

respectively. These energy densities are higher than other reports on MoS_2 nanostructures. The present work suggests that the improved and sustained capacitive performance of device is due to the availability of functional groups and exposed edges due to the well separated sheet in synthesized MoS_2. The high capacitance and energy density of our electrodes suggests their suitability for fast charging and longer discharge time in electronic devices. The MoS_2 nanosheets SSC device with high energy density has also been demonstrated for glowing the LED. This work clearly demonstrates the possibility of real time application of such devices.

5.2.4 MoS_2-rGO Heterostructure Based Solid State Supercapacitors

To examine the combined capacitive behaviour of rGO and MoS_2 nanosheets in their heterostructure, we have investigated the capacitive performance of hydrothermally synthesized MoS_2-rGO heterostructure based SSC device with neutral (PVA-Na_2SO_4) and acidic (PVA-H_2SO_4) electrolytes in voltage range of -0.8 to 0.8 V for neutral and -0.7 to 0.7 V, respectively. **Figure 5.8 (a)** displays the SEM image of synthesized MoS_2-rGO heterostructure used as electrode material in SSC device clearly showing small-wrinkled sheets of MoS_2 dispersed over larger sheets of rGO. **Figure 5.8 (b)** depicts the CV curves for heterostructure based SSC device at varied voltage scan rates from 5 to 100 mV s^{-1} with neutral electrolyte. The CV curves seem to maintain quasi rectangular shape, exhibiting good capacitive behaviour due to the synergistic contributions of MoS_2 and rGO nanosheets. The shape of the CV curves does not change with increasing sweep rates implying good rate capability of SSC device with neutral electrolyte.

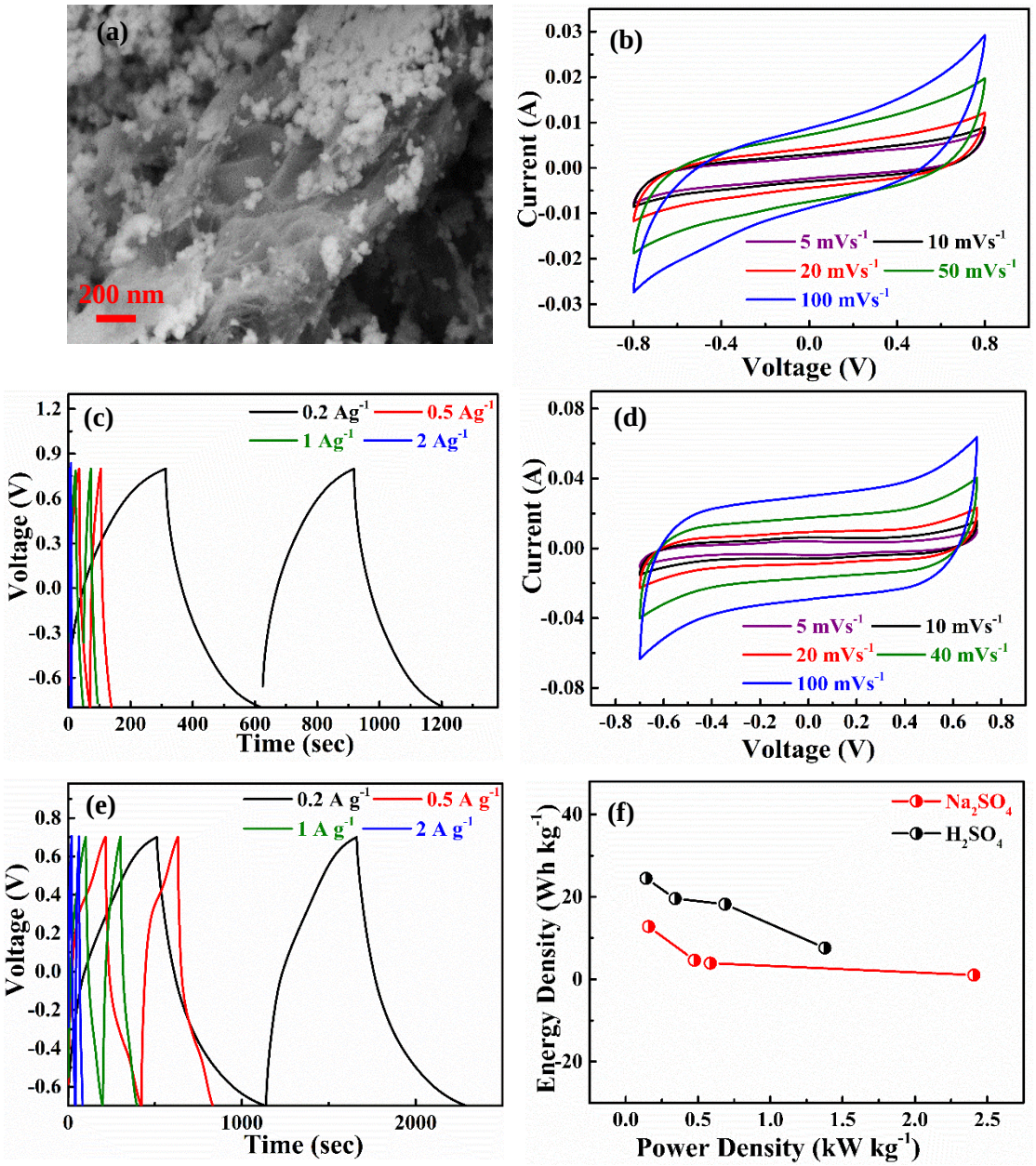

Figure 5.8 *Electrochemical measurements for MoS_2-rGO heterostructure based SSC device (a) SEM image of MoS_2-rGO heterostructure, (b) CV curves at varied sweep rates, and (c) GCD curves at different discharge current densities with neutral electrolyte, (d) CV curves at varied sweep rates, and (e) GCD curves at different discharge current densities with acidic electrolyte, (f) Energy density vs power density plots with both neutral and acidic electrolytes.*

The specific capacitance value of SSC device is estimated using the CV profile and **equation 5.1**. The SSC device shows maximum specific capacitances of 49, 31, 22, 15 and 9 F g^{-1} for full cell at a voltage sweep rates of 5, 10, 20, 50 and 100 mV s^{-1}, respectively. Owing to charge resistive behaviour of MoS_2-rGO heterostructure, a decrease in

capacitance with increased scan rate is observed. The GCD characteristics of SSC device has been carried out for neutral electrolyte at varied current densities from 0.2 to 2 A g^{-1}, as shown in **Figure 5.8 (c)**. The specific capacitance of the SSC device is derived from GCD curve using **equation 5.2**. The maximum specific capacitances of 36, 13, 11 and 3 F g^{-1} are obtained at discharge current densities of 0.2, 0.5, 1 and 2 A g^{-1}. The lower value of specific capacitance with neutral electrolyte can be attributed to dominance of rGO sheets over MoS_2 nanoflowers. **Figure 5.8 (d)** and **(e)** represent capacitive behaviour of SSC device in acidic electrolyte. The CV curves of **Figure 5.8 (d)** show quasi rectangular behaviour, which implies the possibility of cation intercalation and reversible redox reactions at the interface of electrode/electrolyte along with double layer formation. The maximum specific capacitance of 68, 58, 48, 37 and 31 F g^{-1} has been obtained at sweep rate of 5, 10, 20, 50 and 100 mV s^{-1}, respectively, which is higher compared with neutral electrolyte. The GCD curves of SSC with acidic electrolyte are shown in **Figure 5.8 (e)**, which also indicate pseudocapacitive response of SSC device induced by redox reactions contribution at electrode/electrolyte interface. The specific capacitances of 92, 72, 67 and 28 F g^{-1} are obtained at discharge current densities of 0.2, 0.5, 1 and 2 A g^{-1}, respectively. The enhanced capacitance values of MoS_2-rGO heterostructure based SSC device have been obtained with acidic electrolyte compared to neutral electrolyte, which could be due to the dominance of large rGO sheets over MoS_2 nanosheets in heterostructure. Further, energy density (E) and power density (P) of designed heterostructure SSC device are determined using **equations 5.3** and **5.4**. The maximum energy densities of 12.8 and 24.5 W h kg^{-1} are observed at power densities of 0.158 kW kg^{-1} and 0.140 kW kg^{-1} for neutral and acidic electrolytes, respectively. **Figure 5.8 (f)** depicts the high sustainability of energy density of SSC device at higher power densities for both neutral and acidic electrolytes,

which can be attributed to the morphology and functional groups of heterostructure that provide ultrafast transportation of ion between the layers.

The significance of electrode kinetics and interface reaction of SSC device with both electrolytes has been carried out by performing EIS study and corresponding Nyquist plots and equivalent circuit are given in **Figure 5.9 (a)**. It shows the internal resistance, R_s ~ 2.1 Ω and 1.2 Ω, while charge transfer resistance, R_{CT} ~ 590 Ω and 73.6 Ω for SSC device with neutral and acidic electrolytes, respectively. The smaller value of R_{CT} for acidic electrolyte compared to neutral electrolyte suggests ease in electron transfer process at electrode/electrolyte interface with acidic medium.

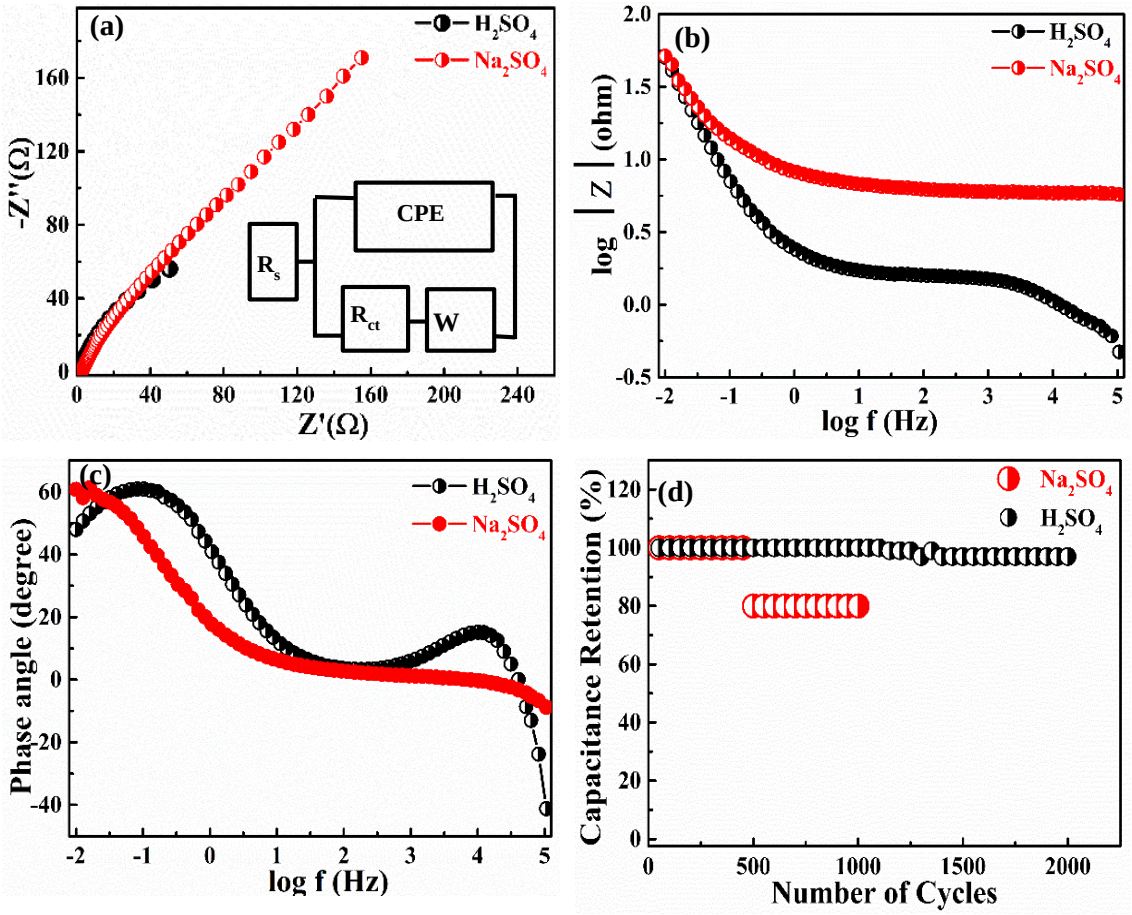

Figure 5.9 *(a) Nyquist plots (inset shows the equivalent circuit), (b) Bode impedance plots, (c) Bode phase angle plots, and (d) Cyclic stability test at discharge current density of 2 A* g^{-1} *for heterostructure based SSC device with both electrolytes.*

Figure 5.9 (b) shows Bode impedance plots, which clearly indicates low value of |Z| for both neutral and acidic electrolyte, suggesting good conducting behaviour of heterostructure device as observed in three cell measurement. The Bode phase plots of **Figure 5.9 (c)** show the maximum phase angle ~60° and 48° for neutral and acidic electrolytes, indicating the presence of pseudocapacitance along with EDLC for SSC devices with both electrolytes. The oxygen containing functional groups are responsible for the Faradaic redox reaction. Additionally, the long-term cycle stability of SSC device is tested for 1000 and 2000 cycles with neutral and acidic electrolytes, respectively, as shown in **Figure 5.9 (d)**. The highest capacitance retentions of ~ 80% and 97% have been observed with neutral and acidic electrolyte, respectively, suggesting higher degree of stability of prepared SSC device with acidic electrolyte.

In summary, we have demonstrated a high capacitive performance of MoS_2-rGO heterostructure based SSC device with both acidic and neutral electrolytes. A higher voltage window and hence higher energy and power densities could be achieved due to the use of a polymer gel-electrolyte in SSC device. The present work suggests the enhancement in capacitive performance of SSC device with acidic solid electrolyte due to the synergetic interaction between rGO and MoS_2, which provide easy intercalation of H^+ ions through the gap of MoS_2-rGO- nanosheets. The presence of rGO in the hybrid material may prevent the MoS_2 nanosheets from clumping together and the high stability of rGO in acidic medium improves the capacitance response of heterostructure based SSC device with acidic electrolyte. We have summarized the capacitive performance of fabricated SSC devices in **Table 5.1**. This research describes an intriguing approach to utilize the MoS_2-rGO heterostructures based SSC device for sustainable development of efficient energy generation and storage devices.

Table 5.1 Capacitive Performance of Fabricated SSC Devices.

Materials	Specific Capacitance ($F\ g^{-1}$) in PVA Na_2SO_4	Specific Capacitance ($F\ g^{-1}$) in PVA H_2SO_4	Energy density ($Wh\ kg^{-1}$) in PVA Na_2SO_4	Energy density ($Wh\ kg^{-1}$) in PVA H_2SO_4	Ref.
rGO-HH	-	35	-	9.5	**Present work**
rGO-Urea	-	27	-	3.8	**Present work**
2H-MoS_2 nanosheets	101	88	36.1	19.6	**Present work**
MoS_2 - nanoflowers	46.5	38	16.4	10	**Present work**
MoS_2-rGO heterostructure	36	92	12.8	24	**Present work**

5.3 Conclusion

In this chapter, we have discussed the capacitive performance for different rGO and MoS_2 nanostructures and their heterostructure based SSC devices. The use of a polymer gel based solid electrolyte allows higher voltage window compared to aqueous electrolyte and hence higher energy densities could be achieved with SSC devices along with other advantages such as better mechanical strength and stability of the SSC device. This study clearly indicates that the rGO based SSC devices show better capacitive response with acidic electrolyte, while MoS_2 nanostructures based SSC devices show better response with neutral electrolyte. The MoS_2 nanosheets based SSC device exhibits the better capacitive response with neutral electrolyte due to the availability of functional groups and exposed edges in well separated sheets of MoS_2. The MoS_2-rGO- heterostructure based SSC device

shows best capacitive performance with acidic solid electrolyte among studied devices due to the dominance of larger dimension rGO nanosheets in heterostructure and the high stability of rGO in acidic medium.